JBMR Plus, 2025, **9**, ziae160
https://doi.org/10.1093/jbmrpl/ziae160
Advance access publication: December 10, 2024
Research Article

Discoidin Domain Receptor 1 impacts bone microarchitecture with aging in female mice

Kimberly Denman[1], Angela Blissett[2], Stevan Glisic[1], Brent Weiss[1], Christina Zachariadou[3], Hani Awad[4,5], Alan Litsky[1], James Cray[6,7,8], Beth S. Lee[9], Brian L. Foster[6], Gunjan Agarwal[10,*]

[1]Biomedical Engineering Department, The Ohio State University, Columbus, OH 43210, United States
[2]Department of Pathology, The Ohio State University, Columbus, OH 43210, United States
[3]Department of Periodontics and Endodontics, School of Dental Medicine, University at Buffalo, Buffalo, NY 14260, United States
[4]Department of Orthopedics, University of Rochester Medical Center, Rochester, NY 14642, United States
[5]Department of Biomedical Engineering, University of Rochester Medical Center, Rochester, NY 14642, United States
[6]Division of Biosciences, College of Dentistry, The Ohio State University, Columbus, OH 43210, United States
[7]Department of Biomedical Education and Anatomy, The Ohio State College of Medicine, Columbus, OH 43210, United States
[8]Division of Orthodontics, College of Dentistry, The Ohio State University, Columbus, OH 43210, United States
[9]Department of Physiology and Cell Biology, College of Medicine, The Ohio State University, Columbus, OH 43210, United States
[10]Department of Mechanical and Aerospace Engineering, The Ohio State University, Columbus, OH 43210, United States
*Corresponding author: Gunjan Agarwal, Department of Mechanical and Aerospace Engineering, The Ohio State University, E503, Scott Laboratory, 201 W19th Ave, Columbus, OH 43210, United States (agarwal.60@osu.edu)

Abstract

Discoidin Domain Receptor 1 (DDR1) is a receptor tyrosine kinase that binds to and is activated by collagen(s), including collagen type I. *Ddr1* deletion in osteoblasts and chondrocytes has previously demonstrated the importance of this receptor in bone development. In this study, we examined the effect of DDR1 ablation on bone architecture and mechanics as a function of aging. Femurs were collected from female global *Ddr1* knockout (KO) and wild-type (WT) mice at 2, 6, and 12 mo of age and analyzed by high-resolution micro-computed tomography (μCT), mechanical testing, and histology. Primary monocytes were collected for in vitro osteoclastogenesis assays. Our studies on younger (2 mo) mice revealed no significant differences between the two genotypes and the microarchitectural and mechanical features had a similar trend as those reported earlier for osteoblast or chondrocyte specific *Ddr1* knockdown. At an advanced age (12 mo), significant differences were noted across the two genotypes. μCT analysis showed a decrease in medullary cavity area as well as increased trabeculation in cortical and trabecular bone in the *Ddr1* KO vs. WT mice. In addition, *Ddr1* KO mouse bones exhibited reduced mechanical properties (lower peak load, yield load, and energy to yield) at 12 mo. Histological analysis revealed reduced osteoclast count in *Ddr1* KO femurs at 12 mo with no significant difference in osteocyte count between the genotypes. In vitro, osteoclastogenesis was impaired in *Ddr1* KO bone marrow derived cells. These results suggest that DDR1 deficiency adversely impacts osteoclast differentiation and bone remodeling in an age-dependent manner.

Keywords: aging, genetic animal model, bone microct, biomechanics, osteoclasts

Lay Summary

Aging leads to bone loss due to imbalance in bone formation and resorption. Bone contains multiple cell types, with the two most important cells for bone maintenance being osteoblasts, which deposit the building material for bone, and osteoclasts, which break down and remove old bone material. Discoidin Domain Receptor 1 (DDR1) is a protein that is present in both osteoclasts and osteoblasts. DDR1 interacts with collagen, the major protein in the bone tissue. The purpose of this research was to discover how DDR1 impacts bone structure and mechanics during aging. Towards this goal, we studied female mice that lacked *Ddr1* gene. Our research showed that the loss of DDR1 causes abnormal bone remodeling and weaker bones with aging. This is likely due to the effect of DDR1 on osteoclasts. Our results suggest that DDR1 could become a potential drug-target to assist individuals with osteoporosis.

Received: May 31, 2024. **Revised:** November 24, 2024. **Accepted:** December 4, 2024

Graphical Abstract

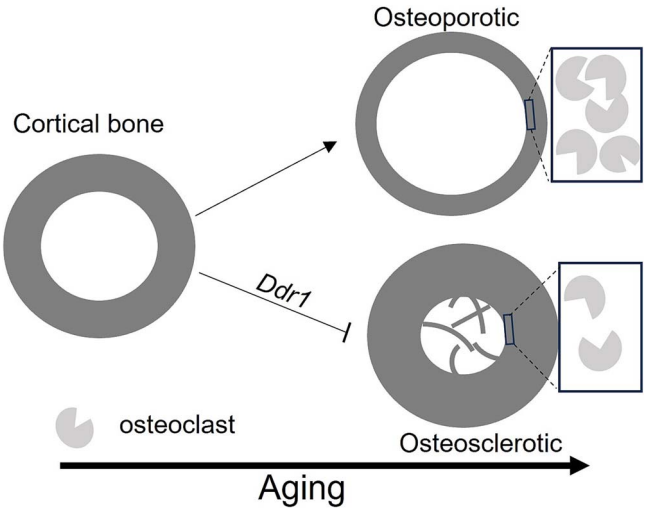

Introduction

Bone tissue is a composite material primarily composed of collagen type I and minerals in the form of hydroxyapatite.[1] Bone remodeling becomes unbalanced with age when the relative rate of bone removal by osteoclasts exceeds the rate of new bone formation by osteoblasts, leading to structural deterioration and increase in bone fragility.[2,3] This disruption in bone homeostasis is in part governed by osteocytes that are known to undergo morphological changes, impaired mechanosensitivty and cell senescence in the aging bone.[4] Unraveling the cellular and molecular mechanisms modulating bone remodeling with aging can help identify new biomarkers or therapeutic targets for age related diseases such as osteoporosis.

Discoidin Domain Receptors (DDR1 and DDR2) are ubiquitously expressed receptor tyrosine kinases that bind to and are activated by collagens.[5] Previous studies by us and others have established how DDR1 plays an important role in modulating collagen type I synthesis,[6] fibrillogenesis,[7,8] fibril structure[9], and vascular calcification.[10] DDR1has also been elucidated to be important for bone development. In an initial study, Vogel et al. reported reduced postnatal growth in global *Ddr1* knockout (KO) mice.[11] Another study of skull morphology analysis by micro-computed tomography (μCT) revealed that *Ddr1* KO mice exhibit proportionally smaller bone size (with no outstanding deformations) as compared to wild-type (WT) mice.[12]

The role of DDR1 in various bone cells has been an active area of interest. By employing inducible deletion of *Ddr1* in chondrocytes, Chou et al. have elucidated how the short stature of *Ddr1* KO mice is likely due to decreased chondrocyte proliferation and apoptosis and delayed endochondral ossification during development.[13] In another study, inducible osteoblast-specific deletion of *Ddr1* also resulted in decreased length of long bones and decreased mineralization in the ribs and sternum, which was associated with reduced osteoblast numbers.[14]While in-vivo studies have elucidated the role of DDR1 in hematopoietic cells like bone-marrow derived macrophages for vascular studies,[15] the role of DDR1 in osteoclasts has thus far been limited to in vitro studies. Osteoclastogenesis (differentiation of bone marrow derived macrophages to osteoclasts), was impaired in the presence of conditioned media obtained from *Ddr1* knockdown in lung cancer cell lines.[16] Conversely, nitrogen-containing bisphosphonates (which inhibit osteoclast activity) have been shown to downregulate *Ddr1*.[17] Imatinib, a clinically used tyrosine kinase inhibitor, (which also inhibits DDR1 activity) has also been reported to inhibit in-vitro osteoclastogenesis.[15,18]

Taken together these studies have provided valuable insights into the role of DDR1 in bone development in multiple cell types; however, much less is understood about the role of DDR1 in the aging bone.[8,10] In this study, we investigated how DDR1 impacts the long bone in aging females by using global *Ddr1* KO mice (2 to 12 mo of age). Towards this goal, we analyzed the microstructural and mechanical properties of femurs, osteocyte and osteoclast numbers, and osteoclastogenesis in vitro. Our studies were centered on female mice as aging studies are easier to conduct with female rodents (which can be group-housed for longer durations without fighting concerns). Recent studies on the role of DDR1 in bone biology have also been limited to female mice[19] as the mutant females have been found to exhibit a greater difference than males when compared to age and sex matched WT animals in earlier studies.[11,14] Further, it is well known that age-related bone loss is exacerbated in females especially after menopause due to enhanced osteoclast activity (resulting from a decrease in estrogen levels).[20,21] Our results indicate an important role of DDR1 in regulating bone properties with aging in female mice.

Materials and methods

Animals

Animal procedures were approved by the Institutional Animal Care and Use Committee of the Ohio State University (Columbus, OH). The *Ddr1* KO mice utilized in this study were generated by Lexicon Pharmaceuticals, Inc (Woodlands, TX) via homologous recombination as described previously.[9,22] Briefly, coding exons 1-3 of *Ddr1* were deleted resulting in gene silencing (NCBI accession NM_007584). Identification of $Ddr1^{-/-}$ homozygous KO, $Ddr1^{+/-}$ heterozygous, and $Ddr1^{+/+}$ WT mice was performed using PCR-based genotyping from tail clippings as described previously.[9] Mice were

housed under a 12-h light/dark cycle and had access to standard rodent chow and water *ad libitum*. Female *Ddr1* KO and WT mice were euthanized at 2, 6, or 12 mo, and femurs were harvested and cleaned of fat and muscle. The number of animals used for each age and genotype ranged from $n = 3$ to 7 and were determined based on our previous study.[22] Left femurs were fixed in formalin and utilized for histology. Right femurs were wrapped in phosphate buffer saline (PBS) soaked gauze and frozen at –20 °C for measurement of structural and mechanical properties.

Micro-computed tomography

Right femurs were scanned in a saline filled chamber using a Skyscan 1172 μCT scanner operating at 50 kV with an isotropic resolution of 10 μm. The exposure time was 260 ms, with 499 projections used for the reconstruction of each slice. All scans were reconstructed with a beam hardening correction of 20% and a ring artifact correction of 4. Each sub-scan was aligned individually to its optimal correction alignment using NRecon software (version, 1.6.1.5; Micro Photonics, Allentown, PA). In order to quantify bone mineral density (BMD) two hydroxyapatite (HA) calibration phantoms with known densities of 250 and 750 mg/cm^3 were used to convert grey-scale levels to HA density values. Phantoms were scanned and reconstructed under identical conditions as test samples. At least $n = 4$ bones were scanned for each genotype and age group.

CTAn (CT Analyser, Skyscan version 1.9) and CTVol software (Skyscan; Bruker, Billerica, MA) was used to render 3D models of trabecular and cortical regions of interest (ROI). Cortical bone ROI was selected with a length 15% of full femur length at the center-most cross-sectional slice in the diaphysis. Trabecular bone ROI was selected as a cylindrical region (1/10th of femur length), beginning a distance of 1.5% full femur length away from the distal growth plate extending towards the diaphysis. The CTAn software "shrink-wrap" feature was used to fit the ROI to the bone perimeter (BP) and 3D models were constructed. Global thresholds were optimized and set at 110-255 for cortical regions and 55-255 for trabecular bone. Morphometric analysis of cortical and trabecular bone was performed to determine tissue volume (TV), bone volume (BV), percent bone area (BV/TV), tissue area (T.Ar), bone area (B.Ar), and bone mineral density (BMD). Additionally, medullary (or marrow) area (M.Ar), cortical area fraction (BAr/T.Ar), average cortical thickness (Ct.Th), and mean polar moment of inertia (MMI) were determined for cortical bone while trabecular number (Tb.N), trabecular thickness (Tb.Th), and trabecular separation (Tb.S) were ascertained for trabecular bone.[23]

Bone biomechanical analysis

Bone biomechanics were analyzed in unfixed right femurs using three-point bend methodology at room temperature. Femurs were placed in an MTS 858 test frame (MTS Corp., Eden Prairie, MN) with a span length of 8.79 mm between the lower supports, and displacement control tests were conducted at 0.5 mm/s on the center of the diaphysis until failure. The load (force) versus displacement curves were recorded for each femur and were utilized to ascertain the yield load and peak (max) load. A linear trendline was applied to the elastic portion of the curve from which stiffness was derived. Energy absorbed was calculated by using a MATLAB script to find the area under the curve until the yield point. A sample size of at least $n = 4$ femurs was used for each genotype and age group.

Histology

Left femurs were fixed in 10% neutral buffered formalin (Fisher Scientific, Kalamazoo, MI) for 48 h, washed twice in PBS and demineralized in 10% EDTA pH 7.4 for 1–2 wk until the tissue was "soft" to the touch. Decalcified samples were washed twice in PBS, transferred to 70% EtOH in labeled histology cassettes and processed with an automatic tissue processor (Tissue-Tek 3-000; Sakura, Torrance, CA, USA or ASP 300; Leica Microsystems, Buffalo Grove, IL, USA). Samples were embedded in paraffin such that cross-sections of the proximal metaphysis and mid-shaft diaphysis, and longitudinal sections of the distal metaphysis to mid-shaft diaphysis, could be acquired. Sections 5-μm-thick were acquired and prior to staining, sectioned tissue samples were deparaffinized in xylene and rehydrated through a graded ethanol series.

To examine osteocyte populations, sectioned tissue samples were subjected to hematoxylin and eosin (H&E) staining. Samples were placed in Harris hematoxylin (Fisher Scientific SH26-500D) for 20 s, rinsed in water, and then placed in eosin Y (Fisher Scientific 22-220-104) for 2 min. The samples were rinsed again, dehydrated through a graded ethanol series, and treated with xylene for 10 min to clear the tissue. Finally, glass coverslips were mounted to the slides using toluene (Fisher Scientific T324-1) and air dried for 24 h. The slides were imaged using a Zeiss Axiovert microscope with a Ziess MRc5 camera at 10×-40× magnification. ImageJ and MATLAB were used to quantify osteocyte numbers and calculate the tissue area.

To examine osteoclast populations, sectioned tissue samples were subjected to tartrate-resistant acid phosphatase (TRAP) staining following manufacturer's instructions (Sigma #387A-1KT). To perform TRAP staining, samples were incubated in a tris base buffer at 37 °C for 1 h and then stained in the staining solution (2% fast garnet/nitrite solution, 1% napthol AS-Bl phosphate solution, 4% acetate solution, and 2% tartrate solution in deionized water (dH_2O) pre-warmed to 37 °C for 60 min in the dark. After staining, the samples were washed in dH_2O and counterstained for 20 s in 1:10 Gill's hematoxylin in H_2O. The samples were rinsed in dH_2O, and glass coverslips were mounted to the slides with ImmunoHistoMount (Sigma I1161). Images were taken with a Zeiss Axiovert microscope with a Ziess MRc5 camera at 10-40× magnification. Stained tissue appeared light brown with purple regions corresponding to TRAP. ImageJ was used to measure the length of TRAP signal along the edge of the bone marrow periphery and the total length of the periphery to quantify the osteoclast perimeter (Oc.P) per BP.

Osteoclastogenesis, in vitro

Primary monocytes were isolated from the murine spleen and bone marrow of 6-mo-old female mice and cultured in-vitro in an osteoclast culture (OC) media to promote osteoclastogenesis. The OC media used comprised of Dulbecco's Modified Eagle Medium (DMEM: Gibco #11995) supplemented with 20% fetal bovine serum (FBS;Gibco #16000-069), 1% penicillin-streptomycin (PS: Gibco #15140-122), 18% L-cell conditioned media (LCMM) and soluble RANKL (PeproTech #315-11). LCMM, which contains secreted mononuclear phagocyte colony-stimulating factor (M-CSF),[24] was

generated by culturing L929 fibroblasts (ATCC #CCL-1) in DMEM, with 10% FBS, and 1% PS. After 5 days of culture, the media were collected, centrifuged to remove cell debris and syringe filtered and stored in –80 °C.

Mononuclear cells were isolated from the spleen by gently layering 4 mL of minced spleen tissue (in DMEM) over 2 mL of Lymphocyte Separation Medium (LSM) in a 15-mL conical tube. Care was taken to not mix the diluted blood into the LSM layer, thus creating a sharp blood-LSM interface. The tube was centrifuged at 440 g for 10 min in order to sediment erythrocytes and polynuclear leukocytes and create a band of mononuclear lymphocytes above the LSM layer. The uppermost layer (corresponding to the mononuclear lymphocytes) was collected and centrifuged at 250 g for 10 min at room temperature. The pellet was re-suspended in OC culture media. In addition, primary monocytes were obtained from bone marrow. Dissected diaphyses of mouse femurs were flushed with DMEM using a syringe and 18G needles. Collected media were centrifuged for 15 min at 250 g and pellet was re-suspended in OC culture media. Monocytes from spleen and bone marrow were pooled together and plated into 100-mm dishes for overnight incubation at 37 °C. Monocytes left in suspension were collected the following day and cell count was established by hematocytometry. Cells were centrifuged at 250 g for 10 min and the cell pellet was re-suspended to an appropriate cell density in OC culture media.

Primary WT and *Ddr1* KO monocytes were plated onto glass coverslips at a density of 500 000 cells/mL. Cells were cultured in OC culture media and analyzed for TRAP staining between 1 and 14 days of culture. Cells became adherent upon differentiation to macrophages and osteoclasts. At selected time points, cell cultures were fixed in 4% paraformaldehyde, washed 1× with PBS and incubated in 50-mM NH_4Cl for 10 min. Permeabilization of cells in 0.1% Triton X-100 was conducted for 15 min after which the samples were incubated with the TRAP staining solution for 50 min at 37 °C in the dark. After staining, the glass coverslips were mounted onto microscope slides and digital images were taken on a Zeiss Axiovert microscope with a Zeiss MRc5 camera and a 20× objective or a 10× objective lens. The number of TRAP positive multinucleated cells and size of differentiated osteoclasts was ascertained using ImageJ. These in-vitro experiments were performed from cells derived from at least $n = 3$ mice for each genotype.

To examine DDR1 expression, a parallel set of cell samples was used for Western blotting. Differentiated osteoclasts from WT mice were lysed and the whole cell lysates were subjected to SDS-PAGE followed by Western blotting onto nitrocellulose membranes. The membranes were probed with primary polyclonal antibody against the DDR1 ectodomain (R&D Systems) and imaged using enhanced chemiluminescence (Amersham Biosciences) after incubation with anti-goat IgG horseradish peroxidase as described earlier.[25]

Statistical analysis

Two-tailed, unpaired *t*-tests with equal variances were used for comparison between genotypes at each age using RStudio© with R version 4.4.1.[26–29] Additionally, data were analyzed for homoscedasticity using Bartlett's test and normality using Shapiro–Wilk's method.[29] For data that were normally distributed and homoscedastic two-way ANOVA was performed, if not a Friedman test was performed in IBM SPSS Statistics version 29. If found significant a post-hoc Scheffe test was executed for parameters that exhibited significance.[30] Significance was determined by $p \leq .05$ and is represented graphically as an exact value for $0.01 \leq p \leq .05$.

Results

Effect of *Ddr1* on bone microarchitecture

Femurs from *Ddr1* KO and WT female mice were analyzed using μCT at 2 (young adult), 6 (mature adult), and 12 mo (middle-aged) to determine the bone microarchitecture. No gross abnormalities were noted in the *Ddr1* KO femurs as compared to WT (Figure 1A), and the differences in femur lengths across the two genotypes were not statistically significant (Table 1). Further, no significant differences were noted between the various cortical bone parameters across the two genotypes at 2 mo of age. However, at 6 mo, several parameters (TV, BV, T.Ar, B.Ar, M.Ar, and MMI) were significantly lower in the cortical bone of *Ddr1* KO mice (Table 1). The lower medullary cavity area (M.Ar) in the KO femurs persisted at 12 mo while other structural parameters were no longer significantly different across the two genotypes at this age. It should be noted that the percent increase in BV and B.Ar between 6 and 12 mo was over two times higher for *Ddr1* KO mice, as compared to WT. Another striking feature was the presence of substantial trabecular bone growth in the medullary cavity of *Ddr1* KO mice at 12 mo, as shown in cross sections of the mid-diaphysis (Figure 1B). Presence of trabecular bone was noted along the entire length of the femur in all 4 of the *Ddr1* KO, but only in 2 of the 5 of aged-matched WT bones (Figure 1C). Quantitative analysis of the cross sections from the center of mid-diaphysis revealed a significant increase in trabecular density in *Ddr1* KO femurs (Figure 1D) along with a decrease in M.Ca (Figure 1E). Analysis of the trabecular bone revealed that the structural parameters were not significantly different between the two genotypes at both 2 and 6 mo of age (Table 2). However, consistent with our observations in the cortical bone, Tb.N was significantly higher in *Ddr1* KO mice at 12 mo (Figure 2A and B). No statistically significant differences in BMD were observed in both the cortical and trabecular bone of the two genotypes across all ages.

Biomechanical properties of long bones in mice lacking *Ddr1*

We used three-point bending to analyze the biomechanical properties of femurs at 2, 6, and 12 mo (Figure 3A). *Ddr1* WT and KO mouse femurs exhibited similar yield load, stiffness, and elastic work to failure (EWF) at 2 mo of age. At 6 mo, *Ddr1* KO femurs exhibited increased stiffness as compared to age matched WT bones. Interestingly, at 12 mo, the femurs from *Ddr1* KO mice had dramatically reduced yield load ($p \leq .001$) and EWF ($p \leq .05$) as compared to age-matched WT (Figure 3B-D). Thus, the two genotypes exhibited different biomechanical profiles with aging. The WT femurs exhibited an increase in yield load, stiffness and EWF with aging, with these biomechanical parameters peaking at 12 mo. However, the KO femurs reached their maximum yield load, stiffness and EWF at 6 mo followed by a sharp decline at 12 mo.

Bone cell populations in long bones

To understand the cellular mechanisms modulating long bone micro-structure and mechanical properties, we examined how lack of *Ddr1* affects bone cell populations. Cortical bone sectioned from the midshaft of the left-side femur and

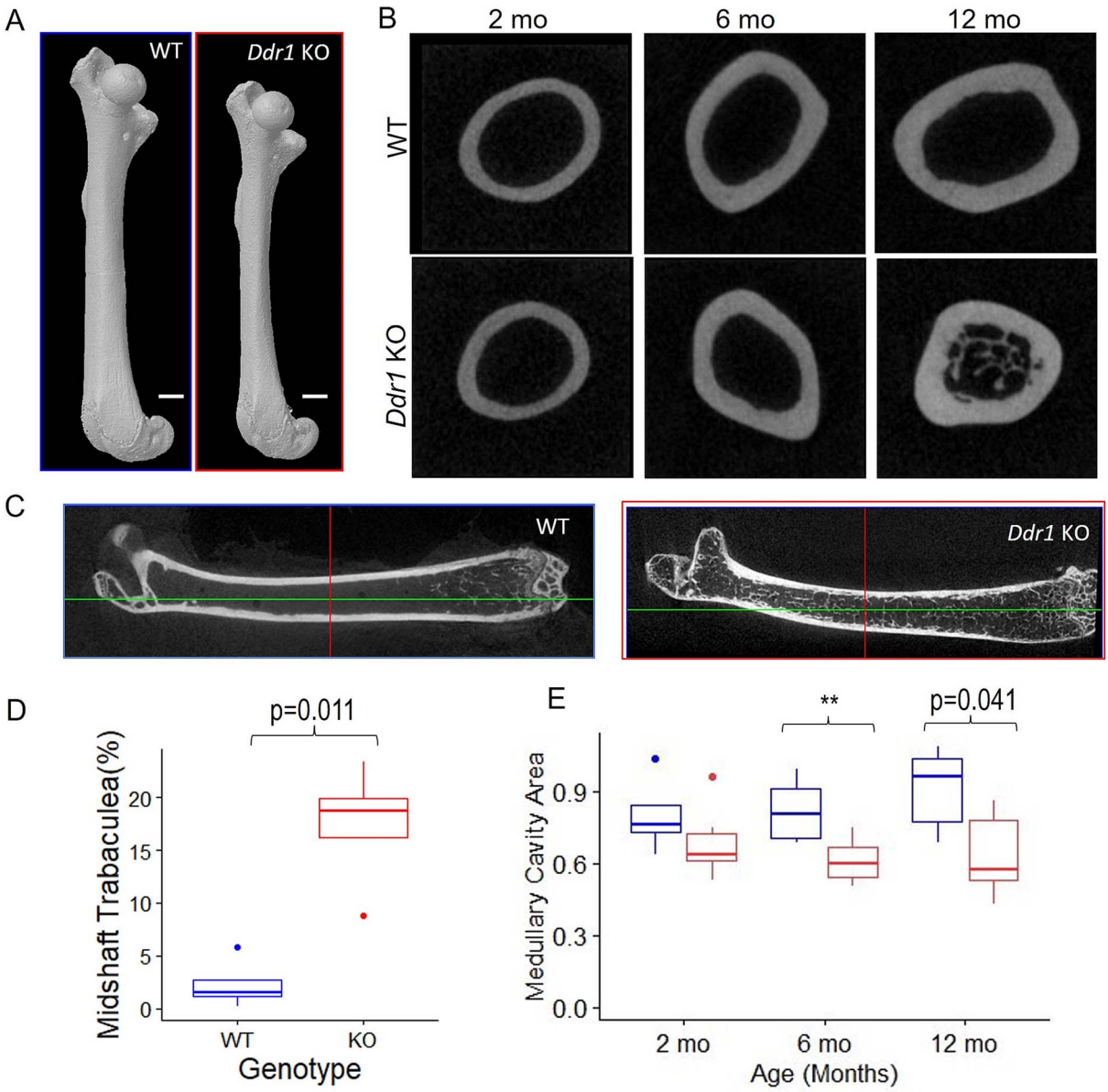

Figure 1. μCT of cortical bone. Representative whole femurs from *Ddr1* KO and WT mice at 2 mo (A). Trabeculae growth was observed in the medullary cavity of 12-mo KO mice, as shown in cross-sections of the mid-femoral diaphysis (B) and longitudinal sections (C) of the murine femur. Quantitative analysis revealed a significant increase of trabecular growth in the mid-shaft cross-sections in 12-mo KO mice (D). The mid-femoral diaphysis also showed a decrease in medullary cavity area in KO femurs at 6 and 12 mo (**$p<.01$) (E). (Number of mice (n) for each group are listed in Table 1). Abbreviations: KO, knockout; μCT, micro-computed tomography; WO, wild-type.

trabecular bone sections from the proximal metaphysis were used to enumerate osteoclasts and osteocytes. The osteocyte count (areal density of osteocyte) was quantified using H&E staining (Figure 4). The osteocyte count in the cortical bone peaked at 6 mo in the WT femurs and was significantly higher than KO. In the trabeculae bone, the osteocyte density monotonically decreased with age in both KO and WT femurs with no statistically significant differences across the two genotypes.

TRAP staining was used to identify osteoclasts. Quantitative assessment of osteoclast count, that is, Oc.P per BP in the cortical bone revealed no significant differences between the genotypes at 2 and 6 mo (Figure 5A and C). However, at 12 mo, the osteoclast count was over two times higher in WT cortical bone as compared to *Ddr1* KO (Figure 5C). This is because the osteoclast count in WT cortical bone significantly increased at 12 mo compared to 2 mo, while no such increase was observed in KO (Table S2). A similar analysis was carried out in the trabecular bone sectioned from the proximal metaphysis of the left-side femur. Overall, TRAP staining was more prominent and TRAP$^+$ cells appeared more plentiful in trabecular bone sections as compared to cortical bone (Figure 5B). However, no significant differences in osteoclast count were noted across the two genotypes at all ages (Figure 5D).

Effect of *Ddr1* ablation on osteoclastogenesis in vitro

To further define the role of *Ddr1* in osteoclasts, primary monocytes isolated from the murine bone marrow and spleen were used to measure osteoclastogenesis in vitro by culturing

Table 1. Structural parameters of cortical bone in mouse femur.

Parameter	2 mo		6 mo		12 mo	
	WT ($n=5$)	KO (8)	WT (6)	KO (6)	WT (5)	KO (5)
Length (mm)	14.20 ± 0.94	13.84 ± 0.40	16.20 ± 0.55	15.85 ± 0.69	16.27 ± 0.77	15.83 ± 0.21
TV (mm^3)	2.96 ± 0.63	2.46 ± 0.43	4.23 ± 0.47	3.33 ± 0.43[a]	4.67 ± 0.93	3.77 ± 0.52
BV (mm^3)	1.24 ± 0.26	1.04 ± 0.15	2.23 ± 0.18	1.87 ± 0.27[a]	2.42 ± 0.43	2.25 ± 0.40
BV/TV (%)	42.04 ± 3.72	42.45 ± 3.65	52.94 ± 2.71	56.34 ± 7.10	52.04 ± 2.16	59.93 ± 9.19
T.Ar (mm^2)	1.38 ± 0.22	1.18 ± 0.18	1.73 ± 0.16	1.39 ± 0.13[a]	1.88 ± 0.31	1.58 ± 0.21
B.Ar (mm^2)	0.58 ± 0.09	0.50 ± 0.06	0.91 ± 0.05	0.78 ± 0.09[a]	0.98 ± 0.14	0.95 ± 0.18
B.Ar/T.Ar	0.42 ± 0.04	0.42 ± 0.04	0.53 ± 0.03	0.56 ± 0.03	0.52 ± 0.02	0.60 ± 0.09
M.Ar (mm^2)	0.80 ± 0.15	0.68 ± 0.13	0.82 ± 0.12	0.61 ± 0.03[a]	0.91 ± 0.17	0.63 ± 0.18[a]
Ct.Th (mm)	0.16 ± 0.02	0.15 ± 0.01	0.21 ± 0.01	0.20 ± 0.02	0.21 ± 0.02	0.20 ± 0.03
MMI (mm^4)	0.21 ± 0.07	0.15 ± 0.04	0.39 ± 0.07	0.27 ± 0.04[a]	0.45 ± 0.14	0.35 ± 0.08
BMD (g/cm^2)	0.69 ± 0.02	0.70 ± 0.02	0.71 ± 0.08	0.75 ± 0.03	0.65 ± 0.14	0.73 ± 0.12

The number (n) of mice examined for each group is indicated. Abbreviations: B.Ar, bone area; BV, bone volume; BMD, bone mineral density; Ct.Th, average cortical thickness; M.Ar, medullary (or marrow) area; MMI, mean polar moment of inertia; T.Ar, tissue area; TV, tissue volume. [a]$p<.05$ across age-matched genotypes.

Table 2. Structural parameters of trabecular bone in mouse femur.

Parameter	2 mo		6 mo		12 mo	
	WT ($n=5$)	KO(8)	WT (6)	KO (6)	WT (5)	KO (4)
TV (mm^3)	0.81 ± 0.06	0.80 ± 0.03	0.93 ± 0.05	0.91 ± 0.04	0.94 ± 0.05	0.90 ± 0.01
BV (mm^3)	0.13 ± 0.07	0.09 ± 0.06	0.11 ± 0.04	0.07 ± 0.10	0.10 ± 0.08	0.12 ± 0.05
BV/TV (%)	16.01 ± 7.92	11.15 ± 6.86	11.73 ± 4.91	7.49 ± 11.06	11.30 ± 8.82	13.77 ± 6.03
Tb.Th (mm)	0.07 ± 0.01	0.07 ± 0.01	0.05 ± 0.01	0.05 ± 0.01	0.06 ± 0.01	0.06 ± 0.01
Tb.N (mm^{-1})	2.29 ± 0.76	1.68 ± 0.94	2.09 ± 0.61	1.38 ± 1.18	1.66 ± 1.03	2.20 ± 0.84[a]
Tb.S (mm)	0.22 ± 0.05	0.29 ± 0.13	0.21 ± 0.04	0.26 ± 0.05	0.28 ± 0.07	0.25 ± 0.07
BMD (g/cm^2)	0.20 ± 0.02	0.19 ± 0.02	0.18 ± 0.04	0.18 ± 0.03	0.15 ± 0.06	0.19 ± 0.05

Abbreviations: BV, bone volume; BMD, bone mineral density; Tb.N, trabecular number; Tb.S, trabecular separation; Tb.Th, trabecular thickness; TV, tissue volume. [a]$p<.05$ across age-matched genotypes.

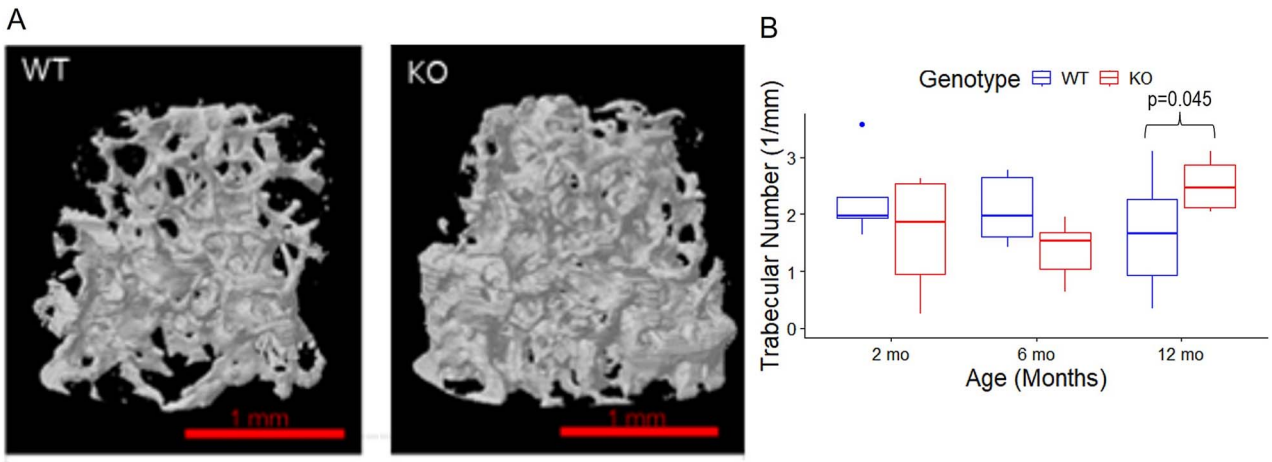

Figure 2. μCT of trabecular bone. 3D reconstruction of trabecular regions of the femur at 12 mo (A) revealed increased trabecular number in 12-mo-old Ddr1 KO femurs as compared to WT (B). (Number of mice (n) for each group are listed in Table 1). Abbreviations: KO, knockout; μCT, micro-computed tomography; WO, wild-type.

them in OC media. The mononuclear cells differentiated and coalesced to form multinuclear osteoclasts, which was monitored via TRAP staining over a span of several days (Figure 6A). The expression of DDR1 in osteoclasts differentiated from WT monocytes was verified using Western blotting (Figure 6B). *Ddr1* KO monocytes exhibited delayed and reduced osteoclastogenesis, which was manifested as smaller size, and fewer number of osteoclasts compared to WT cells at day 10 (Figure 6C and D).

Discussion

In this study, we investigated how deletion of DDR1 impacts the mechanical and microstructural properties of long bones by using *Ddr1* global KO female mice at ages representing young, adult, and middle age. Our investigations revealed that loss of DDR1 impacts bone microarchitecture and mechanics with advancing age. We observed increased trabeculation of marrow space and reduced mechanical properties in femurs of female *Ddr1* KO compared to WT controls at 12 mo. In vitro

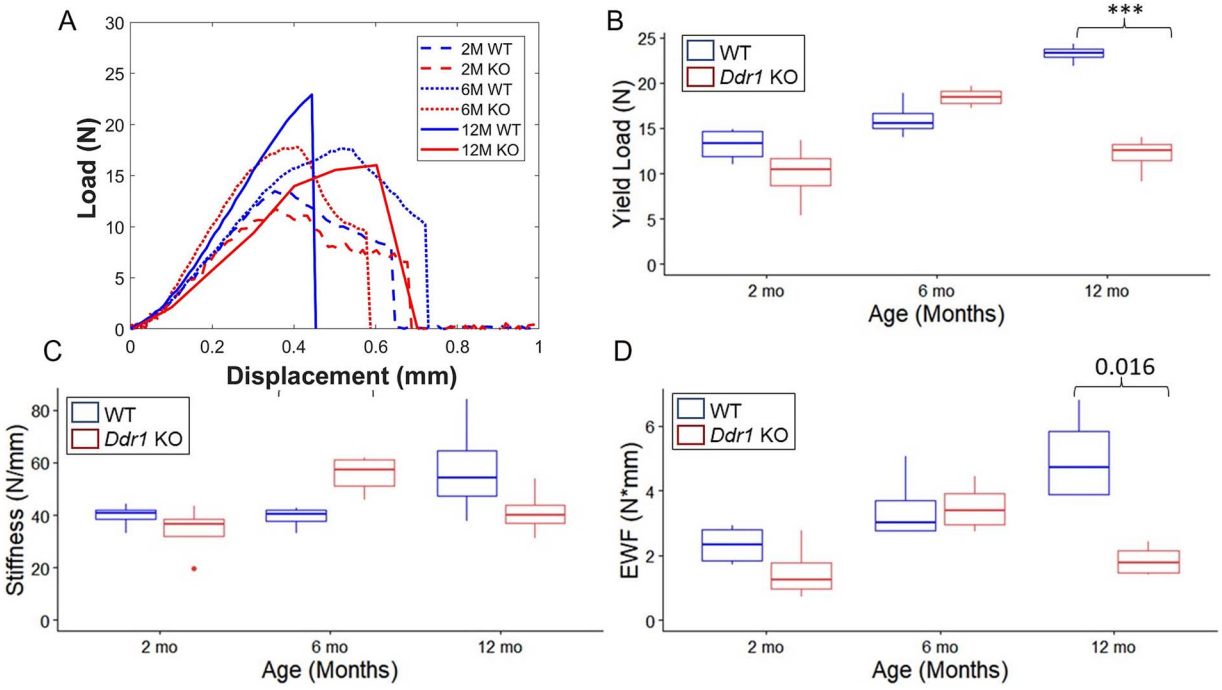

Figure 3. Three-point bending mechanics. Representative three-point bending curves from 2-, 6- and 12-mo-old WT and Ddr1 KO femurs (A). Yield load and stiffness ascertained from three-point bending curves show an age-dependent increase for WT but a sharp decline for KO femurs at 12 mo of age (B, C). The energy to yield load (elastic work to failure) was calculated via the area under the curve and showed a similar trend (D). (*** < .001) Number of mice used for each group was $n = 4$. Abbreviations: KO, knockout; WO, wild-type.

investigations revealed impaired osteoclastogenesis in *Ddr1* KO vs. WT cells. These collective results provide new insights of the functions of DDR1 in bone biology, particularly in the context of aging females.

In our study no significant difference was noted in femur length between the two genotypes across all ages. Previous studies utilizing global and conditional KO mice have indicated that growth curves, especially for females, were more prominently affected upon depletion of DDR1. An early study reported a 35% lower body weight in 2-mo-old female global *Ddr1* KO mice with only a 10% difference between the males.[11] Although femur lengths were not reported in this study, all organs were observed to be proportionately smaller than WT. We note that the mouse model used in this earlier study had deletion of exons 1-12 of *Ddr1* while our model had deletion of exons 1-3, which may partly account for the differences in severity of phenotype. Another study, using chondrocyte specific deletion (CKO) of DDR1[13] also reported reduced body length and mass in 2-mo-old mutant female animals. Femur length was smaller in 1-mo-old mutant mice, with no reports for older animals in this study. Osteoblast specific knockdown (OKO) of DDR1 also resulted in reduced body length and mass with shorter and thinner forelimbs and hindlimbs in 1-mo-old mice (sex not specified).[14] Our analysis was done on $n = 5$-7 femurs from older females (at 2, 6, and 12 mo) which is similar to $n = 6$ to 8 used in previous studies. Taken together, we surmise that although depletion of DDR1 has an effect on early bone development, at the advanced ages used in our study, the growth curves for long bones are no longer significantly different between the two genotypes.

The micro-architectural parameters (obtained using μCT) in our 2-mo-old global *Ddr1* KO had many similarities with those reported for 1- to 3-mo-old OKO and CKO models. All these models showed that depletion of *Ddr1* resulted in reduced tissue area (or bone diameter) in the cortical bone. The trabecular bone in all the three mouse models showed trends to a lower BV/TV and reduced Tb.N as compared to WT in these age groups. Histological analysis revealed a lower osteocyte count in the cortical bone of our global *Ddr1* KO mice at 6 mo, which was consistent with the lower osteoblast count reported in OKO model.[14] These observations collectively reveal that DDR1 in osteoblasts and chondrocytes has an important role in bone formation, which is manifested until adulthood in the female mice.

The mechanical properties of the cortical bone in our global *Ddr1* KO were slightly lower but did not significantly differ from WT mice at 2 mo of age. These differences were more prominent in the *Ddr1* OKO model where a significant decrease in all mechanical parameters was observed at 2 mo[14] (likely due to the decreased cortical thickness and reduced BMD observed in this model). No other age groups have previously been utilized for biomechanical analysis of long bones in *Ddr1* deficient mice. In our study, the long bones from *Ddr1* KO mice exhibited a significant improvement in their mechanical properties between 2 and 6 mo of age, which was not as apparent in the WT bones. In fact, at 6 mo, the *Ddr1* KO femurs had significantly higher stiffness as compared to WT. To ascertain if the increased stiffness corresponds to the brittleness index of the bones, we also analyzed the maximum displacement at yield load and peak load but did not find them to be different across genotypes (data not shown). Cortical thickness and BMD (ascertained using μCT) were also not significantly different across genotypes. The differences in architectural features (lower T.Ar, B.Ar, M.Ar, and MMI in the KO femurs) fail to account for increased stiffness in KO bones. It is interesting to note that such a mismatch between

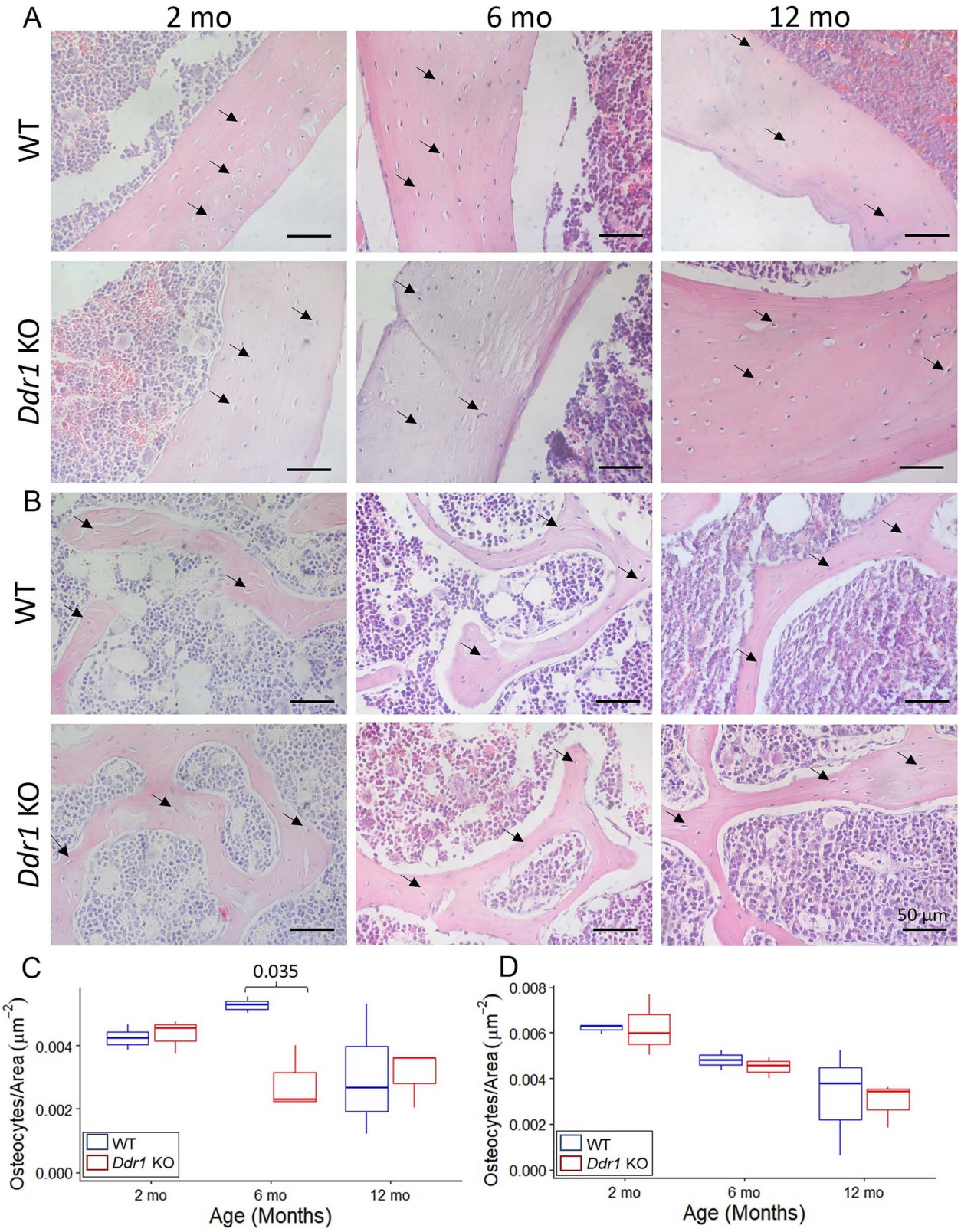

Figure 4. Osteocyte count. Representative H&E images for (A) cortical and (B) trabecular bone were used to ascertain osteocyte count. The osteocyte count per unit area was only found to be significantly higher in the cortical bone of 6-mo-old WT mice (C) and not in the trabecular bone (D). Number of mice used for each group was $n = 3$. Abbreviations: H&E, hematoxylin and eosin; WO, wild-type.

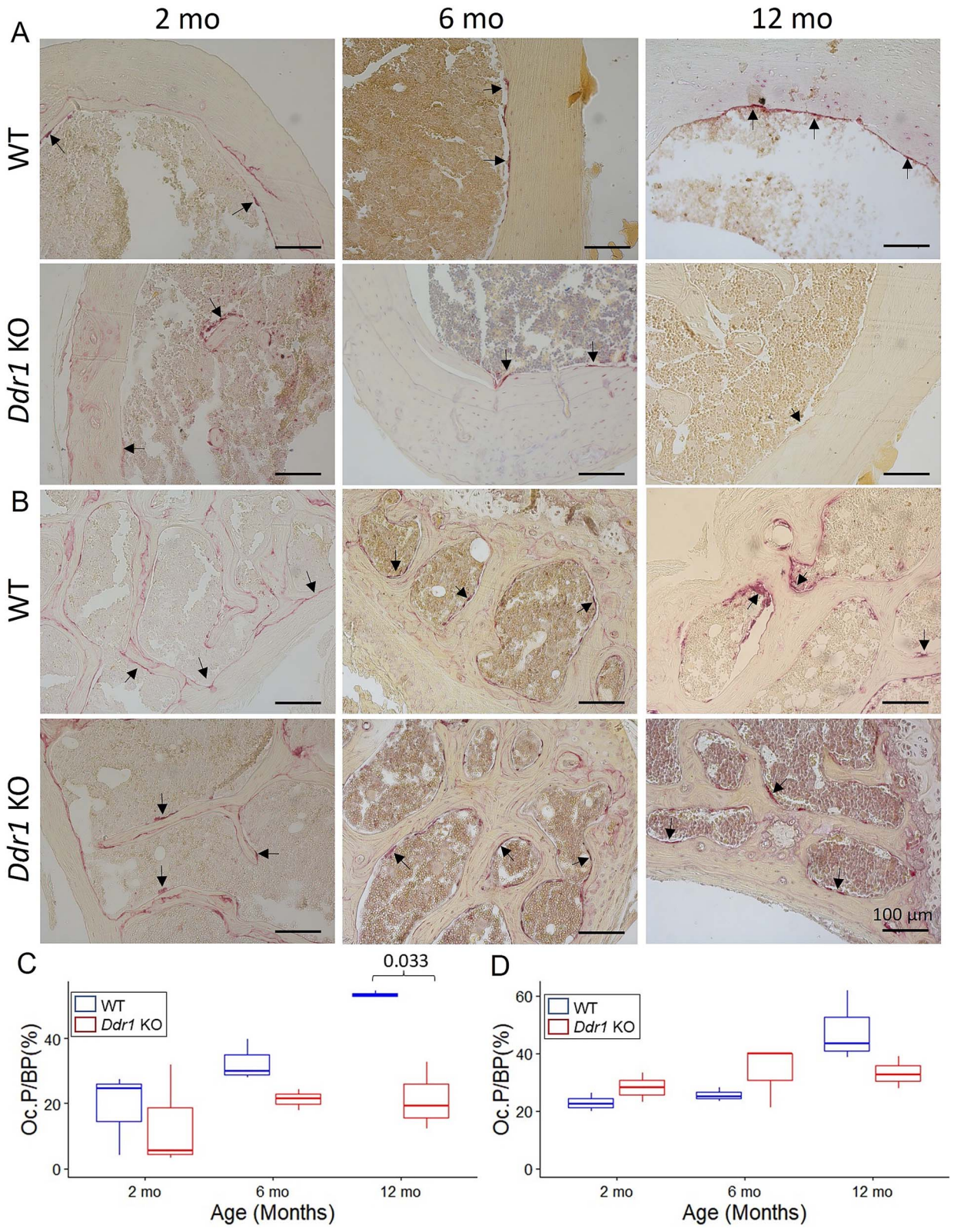

Figure 5. Osteoclast count. TRAP staining of cortical (A) and trabecular bone (B) revealed significantly decreased Oc.P. per BP in the cortical bone (C) at 12 mo but not in the trabecular bone (D). Number of mice used for each group was $n = 3$. Abbreviations: BP, bone perimeter; Oc.P., osteoclast perimeter; TRAP, tartrate-resistant acid phosphatase.

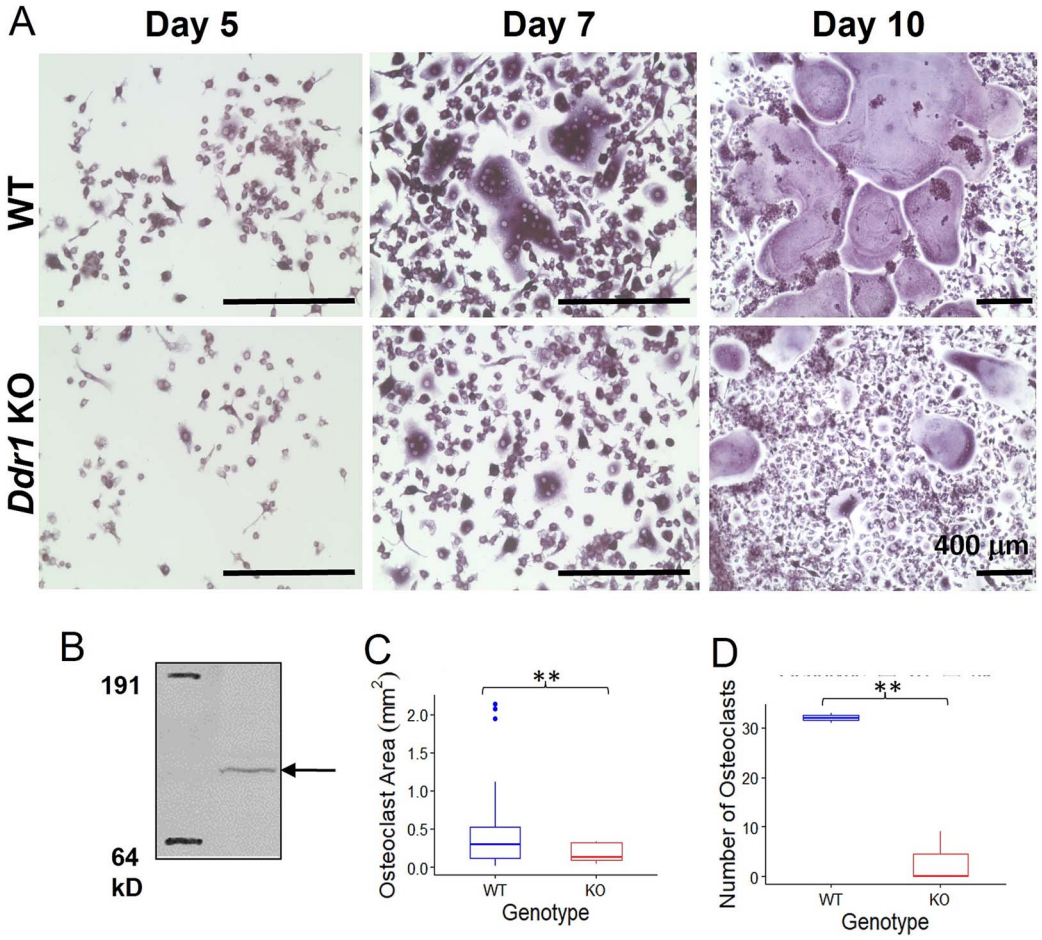

Figure 6. Osteoclastogenesis in vitro. TRAP staining of primary bone marrow cells from 6-mo-old female mice undergoing osteoclastogenesis in vitro (A). Western blot of whole cell lysates from osteoclasts differentiated from WT cells shows Ddr1 expression as a band of ~120 kD (B). Quantitative analysis showed that at day 10, multinucleated giant osteoclasts derived from KO cells were smaller in size (C) and fewer in number (D) as compared to those from WT cells (**$p<.01$). These in-vitro experiments were repeated for cells derived from at least $n=3$ mice per genotype. Abbreviations: KO, knockout; TRAP, tartrate-resistant acid phosphatase; WT, wild-type.

architectural parameters and mechanical properties has also been previously reported in certain rodent models,[31] where it was found that the elastic modulus of the bone tissue material was more aligned with mechanical properties of the femur. Further investigations with more sensitive techniques are underway to ascertain differences in the intrinsic material properties of the bone tissue (eg, the collagen and mineral content, modulus, etc.) which may help explain the anomalous biomechanical properties of 6-mo-old KO femurs.

A key finding of our investigations was that *Ddr1* deletion impacted femur microarchitecture and mechanical properties with advancing age. While peak load, stiffness, and elastic energy of femurs increased from 2 to 12 mo in our WT mice (consistent with earlier age-related studies[32]), *Ddr1* KO mice had a statistically significant reduction in these parameters at 12 mo. Femurs from *Ddr1* KO were mechanically weaker than age-matched WT bones at 12 mo.[14] Interestingly, at this age, all *Ddr1* KO femurs exhibited a decrease in the M.Ar and an in-growth of trabeculation along the entire length of the medullary cavity. Age-related bone loss is known to be more apparent in the trabecular bone with studies reporting reduced trabecular bone in the distal femoral metaphysis of female mice after 2 mo of age.[33] Consistent with this, we noted decreased Tb.N in WT femurs with advancing age, whereas *Ddr1* KO femurs appeared resistant to this bone loss and exhibited an increase in Tb.N at 12 mo as compared to WT. These features mimic some aspects of an osteosclerotic phenotype, where there is more but weaker bone, likely due to osteoclast deficiency or function.[34] Osteopetrosis is one example of an inherited bone disorder characterized by increased bone density but weaker bones due to deficient osteoclast activity.[33] Indeed, our histological analysis revealed reduced osteoclasts in *Ddr1* KO mice at 12 mo, compared to WT mice (where osteoclast numbers consistently increased with age). Experiments to test this effect directly using an in vitro osteoclastogenesis assay revealed that bone marrow derived monocytes from *Ddr1* KO mice showed impaired ability to differentiate to osteoclasts. No significant difference in the osteocyte count was noted across genotypes at 12 mo. Taken together, these results underpin an important role for DDR1 in osteoclastogenesis and bone remodeling with aging in female mice.

Our data support the relevance of *Ddr1* in osteoclasts primarily in older female mice. It is well established that bone loss is exacerbated in menopause, and osteoporosis affects one in three women worldwide and contributes to millions of fractures per year.[35] It should also be noted that age-related diseases such as osteoporosis are characterized by

inflammation, which can regulate osteoclast activity.[36] The removal or inhibition of DDR1 has been shown to decrease inflammatory signals in renal disease, neurodegenerative diseases, and atherosclerosis.[37,38] Thus, attenuation of inflammation with aging may contribute to reduced osteoclast numbers and/or activity in our global *Ddr1* KO mice. Previous studies have postulated *Ddr1* in osteoblasts as a potential target for osteoporosis, as osteoblast specific *Ddr1* conditional knockout mice displayed bone loss and an osteopenia phenotype.[19] Our results elucidate the important and opposing role of DDR1 in the osteoblast-osteoclast axis, which could be equally important to consider if targeting DDR1 function in osteoporosis. Future studies using osteoclast specific knockdown of DDR1 could help further our findings and establish the relevance of DDR1 in clinical osteoporosis. A limitation of our study was that we only used female mice, and it remains to be investigated if these findings hold true for the males.

There are potential mechanisms for how DDR1 may impact osteoclastogenesis and/or osteoclast activity. On the cell-signaling frontier, the Akt pathway is important for cell survival in osteoclasts and initialized by both RANKL-RANK and M-CSF-c-Fms binding.[39,40] DDR1 has been shown to interact with the PI3K/Akt pathway in a variety of cell types and has been shown to stimulate Akt phosphorylation.[41,42] Additionally, DDR1 is also known to interact with the NF-κB pathway in human and murine macrophages,[43,44] a pathway known to be important in osteoclastogenesis. While our current study was largely limited to in-vivo assessment of bone remodeling, future cell-based studies can help elucidate the molecular mechanisms via which DDR1 modulates the various aspects of osteoclast biology. Taken together, our results elucidate the important role of DDR1 in regulating bone microstructure with aging in an osteoclast-dependent manner. These insights provide a more comprehensive understanding of the role of DDR1 in age-related bone remodeling.

Acknowledgments

We also acknowledge Richard Hart, Garrett J. Noble, and Kyle A. Bodnyk for facilitating μCT scans included in the study. Kimberly Denman and Angela Blissett contributed equally to this work.

Author contributions

Kimberly Denman (Conceptualization, Formal analysis, Investigation, Visualization, Writing—original draft, Writing—review & editing), Angela Blissett (Conceptualization, Formal analysis, Investigation, Visualization, Writing—original draft, Writing—review & editing), Stevan Glisic (Data curation, Formal analysis, Investigation, Software), Brent Weiss (Data curation, Formal analysis, Investigation, Software), Christina Zachariadou (Formal analysis, Investigation, Writing—review & editing), Hani Awad (Formal analysis, Investigation, Writing—review & editing), Alan Litsky (Formal analysis, Investigation, Writing—review & editing), James Cray (Formal analysis, Methodology, Supervision, Writing—review & editing), Beth S. Lee (Formal analysis, Methodology, Supervision, Writing—review & editing), Brian L. Foster (Formal analysis, Funding acquisition, Supervision, Writing—review & editing), and Gunjan Agarwal (Conceptualization, Funding acquisition, Project administration, Supervision, Visualization, Writing—original draft, Writing—review & editing).

Supplementary material

Supplementary material is available at *JBMR Plus* online.

Funding

G.A. and B.L.F. were funded by the Ohio State University Center for Medical and Engineering Innovation (CMEI) pilot grant; K.D. and A.B. were funded by graduate fellowships; and G.A. was funded by grant NSF EBMS 2000469 and B.L.F. was funded by grant R01DE027639 from the National Institute of Dental and Craniofacial Research (NIDCR) of the National Institutes of Health (NIH).

Conflicts of interest

None declared.

Data availability

Scripts for R and MATLAB codes will be made available upon request. Supplemental data on statistical analysis is provided in Tables S1 and S2.

References

1. Dempster D, Felsenberg D, Van der Geest S, eds. *The Bone Quality Book: A Guide to Factors Influencing Bone Strength*. Excerpta Medica Elsevier; 2006.
2. Henriksen K, Leeming DJ, Byrjalsen I, et al. Osteoclasts prefer aged bone. *Osteoporos Int*. 2007;18(6):751–759. https://doi.org/10.1007/s00198-006-0298-4
3. Chung P-L, Zhou S, Eslami B, Shen L, LeBoff MS, Glowacki J. Effect of age on regulation of human osteoclast differentiation. *J Cell Biochem*. 2014;115(8):1412–1419. https://doi.org/10.1002/jcb.24792
4. Cui J, Shibata Y, Zhu T, Zhou J, Zhang J. Osteocytes in bone aging: advances, challenges, and future perspectives. *Ageing Res Rev*. 2022;77:101608. https://doi.org/10.1016/j.arr.2022.101608
5. Agarwal G, Smith AW, Jones B. Discoidin Domain Receptors: micro insights into macro assemblies. *Biochim Biophys acta Mol cell Res*. 2019;1866(11):118496. https://doi.org/10.1016/j.bbamcr.2019.06.010
6. Franco C, Ahmad PJ, Hou G, Wong E, Bendeck MP. Increased cell and matrix accumulation during atherogenesis in mice with vessel wall-specific deletion of Discoidin Domain Receptor 1. *Circ Res*. 2010;106(11):1775–1783. https://doi.org/10.1161/CIRCRESAHA.109.213637
7. Agarwal G, Mihai C, Iscru DF. Interaction of Discoidin Domain Receptor 1 with collagen type 1. *J Mol Biol*. 2007;367(2):443–455. https://doi.org/10.1016/j.jmb.2006.12.073
8. Flynn LALA, Blissett ARAR, Calomeni EPEP, Agarwal G. Inhibition of collagen fibrillogenesis by cells expressing soluble extracellular domains of DDR1 and DDR2. *J Mol Biol*. 2010;395(3):533–543. https://doi.org/10.1016/j.jmb.2009.10.073
9. Tonniges JR, Albert B, Calomeni EP, et al. Collagen fibril ultrastructure in mice lacking Discoidin Domain Receptor 1. *Microsc Microanal*. 2016;22(3):599–611. https://doi.org/10.1017/S1431927616000787
10. Ahmad PJ, Trcka D, Xue S, et al. Discoidin Domain Receptor-1 deficiency attenuates atherosclerotic calcification and smooth muscle cell-mediated mineralization. *Am J Pathol*. 2009;175(6):2686–2696. https://doi.org/10.2353/ajpath.2009.080734
11. Vogel WF, Aszódi A, Alves F, Pawson T. Discoidin Domain Receptor 1 tyrosine kinase has an essential role in mammary gland development. *Mol Cell Biol*. 2001;21(8):2906–2917. https://doi.org/10.1128/mcb.21.8.2906-2917.2001
12. Dullin C, Missbach-Guentner J, Vogel WF, Grabbe E, Alves F. Semi-automatic classification of skeletal morphology in genetically altered mice using flat-panel volume computed tomography. *PLoS Genet*. 2007;3(7):e118. https://doi.org/10.1371/journal.pgen.0030118

13. Chou LY, Chen CH, Lin YH, et al. Discoidin Domain Receptor 1 regulates endochondral ossification through terminal differentiation of chondrocytes. *FASEB J*. 2020;34(4):5767–5781. https://doi.org/10.1096/fj.201901852RR
14. Chou L-YY, Chen C-HH, Chuang S-CC, et al. Discoidin Domain Receptor 1 regulates Runx2 during osteogenesis of osteoblasts and promotes bone ossification via phosphorylation of p38. *Int J Mol Sci*. 2020;21(19):1–17. https://doi.org/10.3390/ijms21197210
15. Franco C, Britto K, Wong E, et al. Discoidin Domain Receptor 1 on bone marrow-derived cells promotes macrophage accumulation during atherogenesis. *Circ Res*. 2009;105(11):1141–1148. https://doi.org/10.1161/CIRCRESAHA.109.207357
16. Valencia K, Ormazábal C, Zandueta C, et al. Inhibition of collagen receptor Discoidin Domain Receptor-1 (DDR1) reduces cell survival, homing, and colonization in lung cancer bone metastasis. *Clin Cancer Res*. 2012;18(4):969–980. https://doi.org/10.1158/1078-0432.CCR-11-1686
17. Reel B, Korkmaz CG, Arun MZ, et al. The regulation of matrix metalloproteinase expression and the role of Discoidin Domain Receptor 1/2 signalling in zoledronate-treated PC3 cells. *J Cancer*. 2015;6(10):1020–1029. https://doi.org/10.7150/jca.12733
18. O'Sullivan S, Naot D, Callon K, et al. Imatinib promotes osteoblast differentiation by inhibiting PDGFR signaling and inhibits osteoclastogenesis by both direct and stromal cell-dependent mechanisms. *J Bone Miner Res*. 2007;22(11):1679–1689. https://doi.org/10.1359/jbmr.070719
19. Chou H-C, Lin S-Y, Chou L-Y, et al. Ablation of Discoidin Domain Receptor 1 provokes an osteopenic phenotype by regulating osteoblast/osteocyte autophagy and apoptosis. *Biomedicines*. 2022;10(9):2173. https://doi.org/10.3390/biomedicines10092173
20. Zhen G, Cao X. Bone remodeling and homeostasis. In: *Encyclopedia of Bone Biology (Editor-in Chief: Mone Zaidi)*. Elsevier; 2020;152–161. https://doi.org/10.1016/B978-0-12-801238-3.11180-8
21. Møller AMJ, Delaissé J-M, Olesen JB, et al. Aging and menopause reprogram osteoclast precursors for aggressive bone resorption. *Bone Res*. 2020;8(1):27. https://doi.org/10.1038/s41413-020-0102-7
22. Chavez MB, Kolli TN, Tan MH, et al. Loss of Discoidin Domain Receptor 1 predisposes mice to periodontal breakdown. *J Dent Res*. 2019;98(13):1521–1531. https://doi.org/10.1177/0022034519881136
23. Bouxsein ML, Boyd SK, Christiansen BA, Guldberg RE, Jepsen KJ, Müller R. Guidelines for assessment of bone microstructure in rodents using micro-computed tomography. *J Bone Miner Res*. 2010;25(7):1468–1486. https://doi.org/10.1002/jbmr.141
24. Ladner MB, Martin GA, Noble JA, et al. cDNA cloning and expression of murine macrophage colony-stimulating factor from L929 cells. *Proc Natl Acad Sci USA*. 1988;85(18):6706–6710. https://doi.org/10.1073/pnas.85.18.6706
25. Yeung DA, Shanker N, Sohail A, et al. Clustering, spatial distribution, and phosphorylation of Discoidin Domain Receptors 1 and 2 in response to soluble collagen I. *J Mol Biol*. 2019;431(2):368–390. https://doi.org/10.1016/j.jmb.2018.11.015
26. R Team. *A Language and Environment for Statistical Computing*. R Foundation for Statistical ComputingPublished online 2018:R version 4.4.1. https://doi.org/10.4236/oalib.1107821
27. Fox J, Weisberg S. Visualizing fit and lack of fit in complex regression models with predictor effect plots and partial residuals. *J Stat Softw*. 2018;87(9):1–27. https://doi.org/10.18637/jss.v087.i09
28. Wickham H. *Ggplot2*. Springer International Publishing; 2016. https://doi.org/10.1007/978-3-319-24277-4
29. Fox J, Weisberg S. *An R Companion to Applied Regression*. 3rd ed. SAGE Publications; 2019. https://socialsciences.mcmaster.ca/jfox/Books/Companion/index.html.
30. Signorell A. *DescTools: Tools for Descriptive Statistics*. Published online 2024. Accessed August 2024. https://andrisignorell.github.io/DescTools/.
31. Bozzini C, Picasso EO, Champin GM, Alippi RM, Bozzini CE. Biomechanical properties of the mid-shaft femur in middle-aged hypophysectomized rats as assessed by bending test. *Endocrine*. 2012;42(2):411–418. https://doi.org/10.1007/s12020-012-9616-0
32. Mumtaz H, Dallas M, Begonia M, et al. Age-related and sex-specific effects on architectural properties and biomechanical response of the C57BL/6N mouse femur, tibia and ulna. *Bone Rep*. 2020;12:100266. https://doi.org/10.1016/j.bonr.2020.100266
33. Whyte MP. Osteopetrosis: discovery and early history of "marble bone disease". *Bone*. 2023;171:116737. https://doi.org/10.1016/j.bone.2023.116737
34. Niu Y, Wang Y, Meng H, Yin C, Dang K, Qian A. Biomechanics in clinical application for bone diseases. In: *Bone Cell Biomechanics, Mechanobiology and Bone Diseases*. (Edited by: Airong Qian and Lifang Hu), Elsevier; 2024:315–352. https://doi.org/10.1016/B978-0-323-96123-3.00006-3
35. Who Scientific Group on the assessment of osteoporosis at primary health. In: *Summary Meeting Report Brussels, Belgium, 2004*. 2007: 1–13. WHO Press, Accessed May 2004. http://www.who.int/chp/topics/Osteoporosis.pdf
36. Kamohara H, Yamashiro S, Galligan C, Yoshimura T. Discoidin Domain Receptor 1 isoform-a (DDRla) promotes migration of leukocytes in three-dimensional collagen lattices. *FASEB J*. 2001;15(14):1–23. https://doi.org/10.1096/fj.01-0359fje
37. Franco C, Hou G, Ahmad PJ, et al. Discoidin Domain Receptor 1 (DDR1) deletion decreases atherosclerosis by accelerating matrix accumulation and reducing inflammation in low-density lipoprotein receptor-deficient mice. *Circ Res*. 2008;102(10):1202–1211. https://doi.org/10.1161/CIRCRESAHA.107.170662
38. Fowler AJ, Hebron M, Balaraman K, et al. Discoidin Domain Receptor 1 is a therapeutic target for neurodegenerative diseases. *Hum Mol Genet*. 2020;29(17):2882–2898. https://doi.org/10.1093/hmg/ddaa177
39. Sanjay A, Charles JF. Origin and differentiation of osteoclasts. In: *Encyclopedia of Bone Biology (Editor-in Chief: Mone Zaidi)*. Elsevier; 2020:162–180 https://doi.org/10.1016/B978-0-12-801238-3.11161-4.
40. Kim JH, Kim N. Signaling pathways in osteoclast differentiation. *Chonnam Med J*. 2016;52(1):12–17. https://doi.org/10.4068/cmj.2016.52.1.12
41. Houshdaran S, Zelenko Z, Irwin JC, Giudice LC. Human endometrial DNA methylome is cycle-dependent and is associated with gene expression regulation. *Mol Endocrinol*. 2014;28(7):1118–1135. https://doi.org/10.1210/me.2013-1340
42. Duan X, Xu X, Zhang Y, Gao Y, Zhou J, Li J. DDR1 functions as an immune negative factor in colorectal cancer by regulating tumor-infiltrating T cells through IL-18. *Cancer Sci* Published online August 24. 2022;113:3672–3685. https://doi.org/10.1111/cas.15533
43. Kim S-H, Lee S, Suk K, et al. Discoidin Domain Receptor 1 mediates collagen-induced nitric oxide production in J774A.1 murine macrophages. *Free Radic Biol Med*. 2007;42(3):343–352. https://doi.org/10.1016/j.freeradbiomed.2006.10.052
44. Matsuyama W, Wang L, Farrar WL, Faure M, Yoshimura T. Activation of Discoidin Domain Receptor 1 isoform B with collagen up-regulates chemokine production in human macrophages: role of p38 mitogen-activated protein kinase and NF-κB. *J Immunol*. 2004;172(4):2332–2340. https://doi.org/10.4049/jimmunol.172.4.2332
45. Wickham H, Francois R, Henry L, Muller K, Vaughan D. *dplyr: A Grammar of Data Manipulation*. Published online 2023. R package version 1.1.4. Accessed August, 2024. https://github.com/tidyverse/dplyr.
46. Dorison A, Dussaule J-C, Chatziantoniou C. The role of Discoidin Domain Receptor 1 in inflammation, fibrosis and

renal disease. *Nephron*. 2017;137(3):212–220. https://doi.org/10.1159/000479119

47. Yao Z, Boyce BF. Osteoclast signal transduction pathways: the RANKL/RANK system. In: *Encyclopedia of Bone Biology (Editor-in Chief: Mone Zaidi)*. Elsevier; 2020:200–220 10.1016/B978-0-12-801238-3.62203-1.
48. Lino M, Wan MH, Rocca AS, et al. Diabetic vascular calcification mediated by the collagen receptor Discoidin Domain Receptor 1 via the phosphoinositide 3-kinase/AKT/runt-related transcription factor 2 signaling axis. *Arterioscler Thromb Vasc Biol*. 2018;38(8):1878–1889. https://doi.org/10.1161/ATVBAHA.118.311238

JBMR Plus, 2025, 9, ziae160
https://doi.org/10.1093/jbmrpl/ziae160
Research Article